Measurement and Feedback Driven Entanglement Transition in the Probabilistic Control of Chaos

Thomas Iadecola,[1,2] Sriram Ganeshan,[3,4] J. H. Pixley,[5,6] and Justin H. Wilson[7,8]
[1]Department of Physics and Astronomy, Iowa State University, Ames, Iowa 50011, USA
[2]Ames National Laboratory, Ames, Iowa 50011, USA
[3]Department of Physics, City College, City University of New York, New York, New York 10031, USA
[4]CUNY Graduate Center, New York, New York 10031, USA
[5]Department of Physics and Astronomy, Center for Materials Theory, Rutgers University, Piscataway, New Jersey 08854, USA
[6]Center for Computational Quantum Physics, Flatiron Institute, 162 5th Avenue, New York, New York 10010
[7]Department of Physics and Astronomy, Louisiana State University, Baton Rouge, Louisiana 70803, USA
[8]Center for Computation and Technology, Louisiana State University, Baton Rouge, Louisiana 70803, USA

(Received 29 August 2022; revised 9 February 2023; accepted 20 July 2023; published 8 August 2023)

We uncover a dynamical entanglement transition in a monitored quantum system that is heralded by a local order parameter. Classically, chaotic systems can be stochastically controlled onto unstable periodic orbits and exhibit controlled and uncontrolled phases as a function of the rate at which the control is applied. We show that such control transitions persist in open quantum systems where control is implemented with local measurements and unitary feedback. Starting from a simple classical model with a known control transition, we define a quantum model that exhibits a diffusive transition between a chaotic volume-law entangled phase and a disentangled controlled phase. Unlike other entanglement transitions in monitored quantum circuits, this transition can also be probed by correlation functions without resolving individual quantum trajectories.

DOI: 10.1103/PhysRevLett.131.060403

The dynamics of quantum many-body systems hosts phenomena usually inaccessible to the classical world. In particular, the measurement and control of such systems enables quantum technologies such as efficient state preparation [1–4], quantum error correction [5,6], and nondestructive measurements [7,8]. Enriching unitary dynamics with such nonunitary operations has also led to the discovery of entanglement phase transitions arising from competition between entangling unitary dynamics and projective local measurements [9–12].

The measurement-induced phase transition (MIPT) in its original formulation entails a fundamental change of entanglement scaling from volume law to area law that is connected to percolation [11,13,14], but it has grown past that paradigm [14–57]. While numerous incarnations of the transition exist, it can only be witnessed by quantities that are nonlinear in the density matrix; correlation functions averaged over measurement outcomes are unaffected by the local measurements in the long-time limit. This makes observing MIPTs in experiment a significant challenge requiring either postselection or decoding.

However, augmenting each local measurement with control [58,59] (i.e., unitary feedback conditioned on the measurement outcome) could stabilize a dynamical phase transition that is observable in quantities that are linear in the density matrix. In this work, we identify such a control transition in an open quantum many-body system. Unlike previously studied MIPTs, incorporating local feedback leads to a unique control transition visible in both entanglement measures and correlation functions, making it observable using current experimental setups.

The central idea stems from classical dynamical systems, where methods to control chaotic dynamics have been developed [60–63]. We focus on *probabilistic control* [61–63], which entails the coupled stochastic action of a chaotic map (with probability $1-p$) and a control map (with probability p). These two maps share a periodic orbit, unstable for the chaotic map and stable for the control map. Under the combined stochastic map, the periodic orbit becomes the global attractor at some critical control rate p_{ctrl}. *Prima facie*, this control transition mirrors aspects of MIPTs, albeit at a purely classical level, with the control map as a classical proxy for quantum measurements. The question then arises of whether we can construct a quantum version of probabilistic control transitions and contrast these with quantum MIPTs.

In this Letter, starting from a classically chaotic map with a control transition, we construct a quantum model involving measurements and feedback in which the control transition is enriched by quantum entanglement. The phase transition in the quantum model can be probed by a local order parameter, and is diffusive with dynamic exponent $z \approx 2$ and correlation length exponent $\nu \approx 1$, similar to the classical case. Further, the transition is observed in

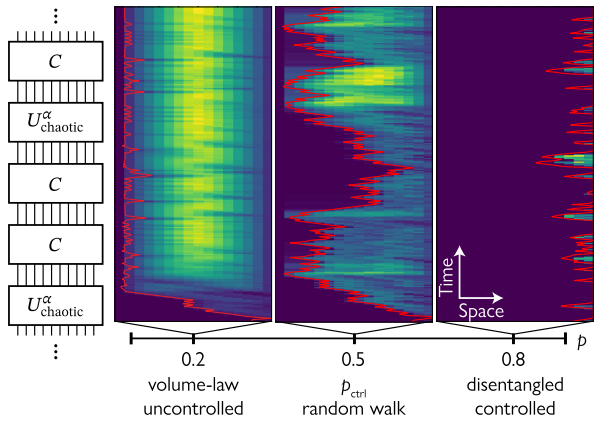

FIG. 1. Control transition. The quantum transition is seen in the dynamics of single trajectories, shown above for $L = 16$. Left: a realization of the stochastic quantum circuit composed of unitary dynamics $U^{\alpha}_{\text{chaotic}}$ and a nonunitary control map C. Right: the phase diagram as a function of the control probability p (black horizontal line). For $p < p_{\text{ctrl}}$, the domain wall between controlled and uncontrolled regions (red) is swept left; entanglement (color scale with brighter colors indicating higher entanglement) grows behind it in a volume-law fashion. For $p > p_{\text{ctrl}}$, the domain wall is pinned to the right edge, and the region to its left is controlled and disentangled. At $p = p_{\text{ctrl}}$, the domain wall undergoes an unbiased random walk and the entanglement grows to an $O(1)$ value.

entanglement and purification measures traditionally used to diagnose MIPTs. In contrast to feedback-free MIPTs, the entanglement entropy grows diffusively at the transition before saturating to an area-law value. Many properties of the transition are understood through the dynamics of an emergent semiclassical domain wall, which undergoes an unbiased random walk at the transition [64]; see Fig. 1.

Model.—We consider a control transition in the classical Bernoulli map [67], given by

$$x \mapsto 2x \mod 1, \tag{1}$$

for $x \in [0, 1)$. Any rational number $x_0 = a/b$ undergoes a finite-length periodic orbit; for instance, $x_0 = 1/3 \mapsto x_1 = 2/3 \mapsto x_0$ is a periodic orbit of length 2. However, since the rational numbers are a set of measure zero in the interval [0, 1), almost every initial state undergoes chaotic dynamics. To control this dynamics onto a periodic orbit of our choosing (with points $\{x_j\}$), we define connected regions Δ_j such that $x_j \in \Delta_j$ and $\cup_j \Delta_j = [0, 1)$, yielding the control map [61]

$$x \mapsto (1 - a)x_j + ax \quad \text{if } x \in \Delta_j. \tag{2}$$

Note that x_j are attractive fixed points of the control map for $|a| < 1$. We consider a stochastic dynamics which, at each time step, applies the chaotic map [Eq. (1)] with probability $1 - p$ and the control map [Eq. (2)] with probability p. For a critical control rate p_{ctrl}, there is a phase transition, with properties that are known exactly [62,64], between an uncontrolled phase where the system never reaches the periodic orbit and a controlled phase where it always reaches the orbit.

To build a quantum model, we map the above to qubits as follows. Write $x \in [0, 1)$ in base 2 as $x = 0.b_1b_2b_3\cdots$ where $b_i \in \{0, 1\}$. The Hilbert space is then spanned by computational basis (CB) states $|b_1b_2b_3\cdots\rangle \equiv |x\rangle$. Now, $|2x \mod 1\rangle = |b_2b_3b_4\cdots\rangle$, i.e., Eq. (1) implements a leftward shift of the bitstring. Next, we truncate the Hilbert space to bitstrings of length L and implement Eq. (1) via the unitary operator

$$T|b_1b_2\cdots b_L\rangle = |b_2b_3\cdots b_Lb_1\rangle, \tag{3}$$

which is identical to Eq. (1) up to an error $O(2^{-L})$. However, in this formulation, every initial state belongs to a periodic orbit of length $\leq L$. To restore a notion of chaos in the thermodynamic limit $L \to \infty$ requires the typical orbit length to be exponential in L [68–70]. To accomplish this, we compose Eq. (3) with a scrambling operation S_α on the last few qubits. We consider two options for S_α: a "classical" ($\alpha = \text{cl}$) and a "quantum" ($\alpha = \text{qm}$) one. The former acts as a permutation on the eight-dimensional space of bitstrings $b_{L-2}b_{L-1}b_L$, while the latter is a Haar-random unitary acting on the last 2 qubits. The chaotic unitary is then

$$U^{\alpha}_{\text{chaotic}} = S_\alpha T. \tag{4}$$

The unitary map $U^{\text{cl}}_{\text{chaotic}}$ is classical in that it maps CB states to CB states—it is a reversible cellular automaton (CA). We choose S_{cl} such that $U^{\text{cl}}_{\text{chaotic}}$ is a chaotic CA with typical orbit length $e^{O(L)}$ [64]. This construction mimics the dynamics of a dense subset of the real numbers, called normal numbers [71], that can rigorously be shown to recover the ergodic behavior of the Bernoulli map [64]. Contrariwise, $U^{\text{qm}}_{\text{chaotic}}$ generates chaotic quantum dynamics in the sense that an initial CB state develops volume-law entanglement in $O(L^2)$ time owing to the locality of the scrambler S_{qm} [64]. Crucially, in the quantum-chaotic implementation the dynamics is no longer that of a single bitstring, but rather of an entangled superposition of such strings and hence no longer corresponds to the representation of a single number.

We implement the (inherently nonunitary) control map via measurement and feedback. We choose the period-2 orbit $\{x_0 = 1/3, x_1 = 2/3\}$ and $a = 2^{-1}$ in Eq. (2). For this a, the classical control transition occurs at $p_{\text{ctrl}} = 0.5$ [62]. We then break up the control map,

$$C = A_{\text{ctrl}}T^{-1}R_L, \tag{5}$$

into the multiplication $|x\rangle \mapsto |2^{-1}x\rangle$ ($T^{-1}R_L$) followed by the addition $|2^{-1}x\rangle \mapsto |2^{-1}x + 2^{-1}x_j\rangle$ (A_{ctrl}). R_L projectively measures qubit L in the CB and flips it if the outcome is $|b_L\rangle = |1\rangle$:

$$R_L|\psi\rangle = \begin{cases} \frac{P_L^0|\psi\rangle}{\|P_L^0|\psi\rangle\|} & \text{with probability } \|P_L^0|\psi\rangle\|^2, \\ \frac{X_L P_L^1|\psi\rangle}{\|P_L^1|\psi\rangle\|} & \text{with probability } \|P_L^1|\psi\rangle\|^2, \end{cases} \tag{6}$$

where P_L^0 and P_L^1 project the Lth qubit onto $|0\rangle$ and $|1\rangle$, respectively, and X_L is the Pauli-X operator at site L. Subsequently, $T^{-1}|b_1 b_2 \cdots b_{L-1} 0\rangle = |0 b_1 b_2 \cdots b_{L-1}\rangle$ completes the multiplication operation. Finally, we apply the controlled adder circuit

$$A_{\text{ctrl}}|x\rangle = \begin{cases} |x + 0.00101\ldots011\rangle & \text{if } b_2 = 0 \\ |x + 0.01010\ldots101\rangle & \text{if } b_2 = 1 \end{cases}, \tag{7}$$

which can be built from local unitary operations as described in the Supplemental Material [64]. The conditional on b_2 determines whether to push CB states $|x\rangle$ toward $|x_0\rangle$ or $|x_1\rangle$.

The stochastic dynamics at each time step is generated by $U^{\alpha}_{\text{chaotic}}$ with probability $1-p$ and C otherwise. When the chaotic dynamics is generated by $U^{\text{cl}}_{\text{chaotic}}$, this dynamics occurs in the space of CB states, and is therefore equivalent to a probabilistic cellular automaton; the dynamics is classical, despite being phrased quantum mechanically. For $U^{\text{qm}}_{\text{chaotic}}$, the chaotic dynamics becomes entangling, and C disentangles the system by pushing it toward the periodic orbit of the underlying classical model. These dynamics can be formulated as a quantum channel; with additional dephasing, the superoperator that evolves the average density matrix reduces to the Frobenius-Perron evolution operator for classical phase space distributions [64].

Classical transition.—Our first order of business is to show that the classical control transition survives the above mapping to qubits. To characterize the transition, we first note that the orbit $\{x_0 = 1/3, x_1 = 2/3\}$ is a two-dimensional subspace spanned by the CB states $|1/3\rangle = |0101\cdots01\rangle$ and $|2/3\rangle = |1010\cdots10\rangle$. Thus, the control map [Eq. (2)] steers the system's dynamics onto Néel-ordered antiferromagnetic states. We probe this order using the order parameter

$$\mathcal{O} = -\frac{1}{L}\sum_{i=1}^{L} Z_i Z_{i+1}, \qquad Z_{L+1} \equiv Z_1, \tag{8}$$

where Z_i is the Pauli Z operator for bit i [$Z_i|b_i\rangle = (-1)^{b_i+1}|b_i\rangle$]. The two Néel states maximize $\langle\mathcal{O}\rangle = 1$, so the controlled phase can be viewed as an ordered phase characterized by $\langle\mathcal{O}\rangle \to 1$ in the thermodynamic limit. To probe the transition into the ordered phase

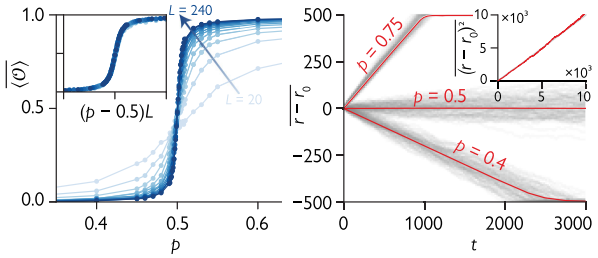

FIG. 2. Classical transition. Left: realization-averaged order parameter $\overline{\langle\mathcal{O}\rangle}$ for various system sizes. The crossing near $p = 0.500(1)$ is where the transition occurs. Inset: collapse indicates that $\nu = 1.00(2)$. Right: the position of the FDW initialized at $L/2$ for $L = 1000$ in the controlled phase ($p = 0.75$), the uncontrolled phase ($p = 0.4$), and at the transition ($p = 0.5$). Gray curves are all 1000 realizations, and red curves are averages. Inset: at $p = 0.5$ we see random walk behavior in 4 orders of magnitude for $r^2 = t$, and a fit confirms $z = 2.04(8)$.

in the classical case, we simulate the dynamics of CB states under the stochastic action of $U^{\text{cl}}_{\text{chaotic}}$ and C out to $2L^2$ time steps for a range of p and L. For each p and L, we calculate $\langle\mathcal{O}\rangle$ at the final time, and average the result over 1000 randomly chosen initial states and circuit instances. We refer to this realization-averaged quantity as $\overline{\langle\mathcal{O}\rangle}$. Our results, shown in Fig. 2 (left), show that Néel order develops for $p \gtrsim 0.5$. Scaling collapse with an ansatz $\overline{\langle\mathcal{O}\rangle} = f[L^{1/\nu}(p - p_{\text{ctrl}})]$ is consistent with a transition point $p_{\text{ctrl}} = 0.500(1)$, coinciding with the known result for Eqs. (1) and (2) [62], and with a correlation length critical exponent $\nu = 1.00(2)$ that also agrees with analytic results for the classical transition [62,64]. (For details on our scaling collapse methodology and further comparison with the classical map and control transition studied in Refs. [61,62], see the Supplemental Material [64].) Additionally, the fluctuations of $\langle\mathcal{O}\rangle$ over realizations peak at $p = 0.5$ (not shown), serving as another indicator of the transition.

To further characterize the control phase transition, we consider the behavior of the "first" (i.e., leftmost) Néel domain wall in the chain—for example, the first domain wall (FDW) in the following configuration is highlighted with a box: $|01010\boxed{11}0110\ldots\rangle$. The position of the FDW bounds the distance from a point $x \in [0, 1)$ to the periodic orbit: if the FDW is on the rth bond in the chain, then $\min_j |x - x_j| \lesssim O(2^{-r})$ for $j = 0, 1$. The FDW thus constitutes the boundary between controlled and uncontrolled regions of the qubit chain; see Fig. 1. We simulate the dynamics of the FDW when initialized at $r_0 = L/2$ and find averaged displacement and mean-squared displacement consistent with a random walk with bias $2p - 1$ [see Fig. 2 (right)]:

$$\overline{\langle r - r_0\rangle} = (2p-1)t, \qquad \overline{\langle (r-r_0)^2\rangle}|_{p=0.5} = t. \tag{9}$$

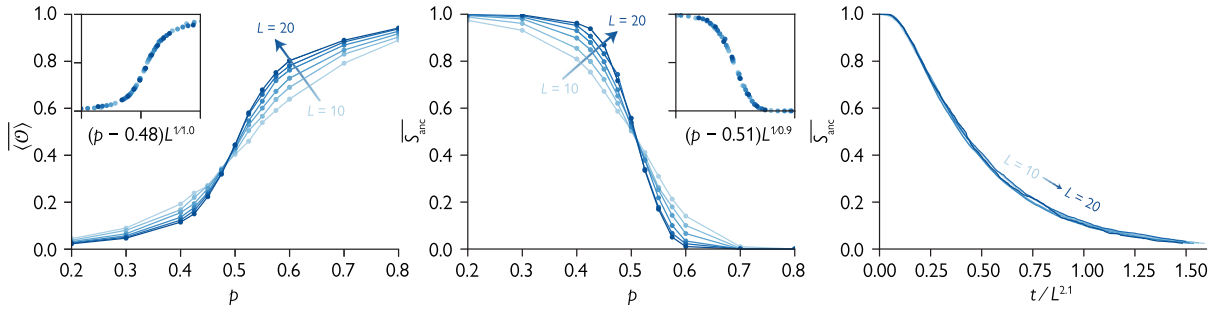

FIG. 3. Quantum transition. Left: Order parameter $\langle\mathcal{O}\rangle$ at $t = 2L^2$ averaged over initial states and circuit realizations. Inset: scaling collapse assuming $\nu = 1.0(1)$ and $p_{\mathrm{ctrl}} \approx 0.48(1)$. Middle: ancilla entanglement order parameter S_{anc} (in units of $\ln 2$) at time $L^2/2$ averaged over initial states and circuit realizations. Inset: scaling collapse assuming $\nu = 0.9(1)$ and $p_{\mathrm{ctrl}} \approx 0.51(1)$. Right: dynamics of $\overline{S_{\mathrm{anc}}}$ collapsed as a function of rescaled time t/L^z near the control transition ($p = 0.5$) with $z = 2.1(1)$. Data are averaged over 2000 realizations for $L = 10, \ldots, 16$, and 1000 realizations for $L = 18$, 20. (For $\overline{S_{\mathrm{anc}}}$ data, 500 realizations are used for $L = 20$.) All points have error bars indicating standard error of the mean; where not visible, they are smaller than the points.

Fitting $\overline{\langle(r - r_0)^2\rangle} \sim t^{2/z}$ at $p = 0.5$ confirms that $z = 2.04(8)$, consistent with an unbiased random walk and with exact results for the original Bernoulli map [62,64]. Thus, our finite size bit string representation of the control transition in the Bernoulli map preserves the universality class of the transition.

Quantum transition.—Next, we examine the fate of the control transition when the classical scrambler S_{cl} is replaced by the Haar-random scrambler S_{qm}. Since the hybrid control circuit [Eq. (2)] distributes over superpositions of CB states, we hypothesize that the control transition survives. Then, above some critical p, the control circuit drives the system to a disentangled state with $\langle\mathcal{O}\rangle \to 1$ as $L \to \infty$, while below this critical value the system enters a volume-law entangled steady state with $\langle\mathcal{O}\rangle \to 0$ as $L \to \infty$. Thus, in addition to a control transition, we expect to see an entanglement transition along the lines of those encountered in feedback-free MIPTs, but with a distinct universality class.

Exact numerical results confirm this simple picture. Figure 3 (left) shows the realization-averaged order parameter $\overline{\langle\mathcal{O}\rangle}$ as a function of p. $\langle\mathcal{O}\rangle$ is measured at $t = 2L^2$ to ensure that the system reaches a steady state [64]. Similar to the classical case, there is a crossing near $p = 0.5$. The inset of Fig. 3 (left) shows a scaling collapse assuming $\nu = 1.0(1)$ and $p_{\mathrm{ctrl}} = 0.48(1)$, suggesting a control transition near the expected location. In the Supplemental Material, we show that the fluctuations over realizations of $\langle\mathcal{O}\rangle$ peak at $p = 0.5$, similar to the classical transition.

We further investigate this transition using tools developed for MIPTs. Certain MIPTs are viewed as purification transitions with one phase able to purify mixed states in a finite time [15]. This purification transition is probed by preparing the system in a maximally entangled state with one ancilla qubit and tracking the ancilla's entanglement entropy S_{anc} as a function of time [72] for varying L and p. At the purification transition, we expect a crossing of the $\overline{S_{\mathrm{anc}}}$-vs-$p$ curves for different L at times of order L^2; Fig. 3 (middle) shows this crossing near $p = 0.5$ with the inset showing data collapse assuming $\nu = 0.9(1)$ and $p_{\mathrm{ctrl}} = 0.51(1)$. These data are taken after evolving the system for a time $t = L^2/2$, but the results are insensitive to small variations of this hyperparameter. To characterize the quantum dynamics at the transition, we consider $\overline{S_{\mathrm{anc}}}(t)$ in Fig. 3 (right) at $p = 0.5$. We find that the curves for various L nearly collapse upon rescaling $t \to t/L^z$ with $z = 2.1(1)$, consistent with the dynamical exponent of the classical transition.

Another perspective on MIPTs is that they constitute a volume-to-area-law transition in the entanglement entropy of a pure state. In Fig. 4, we show that the system's entanglement entropy is also sensitive to the control transition. We calculate the von-Neumann entanglement entropy of the half chain, S_A, taking region A to be the leftmost $L/2$ sites of the chain. In Fig. 4 (left) we show $\overline{S_A}$

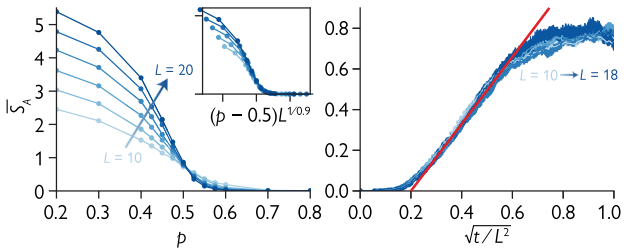

FIG. 4. Entanglement structure and dynamics. Left: realization-averaged von-Neumann entanglement entropy $\overline{S_A}$ at time $2L^2$ for various L and p. At large p $\overline{S_A}$ decreases with L, while at small p it increases linearly with L. There is a crossing near $p = 0.5$, suggesting area-law entanglement at the transition. Inset: scaling collapse of $\overline{S_A}$ assuming $\nu = 0.9(4)$ and $p_{\mathrm{ctrl}} = 0.50(2)$. The data collapse near and above the control transition. Right: $\overline{S_A}$ as a function of rescaled time $\sqrt{t/L^2}$ near the quantum transition ($p = 0.5$). The entanglement dynamics nearly collapse, and there is an intermediate-time regime where $\overline{S_A} \sim \sqrt{t}$ (red line).

as a function of p for different L, finding that it increases with L for $p \lesssim 0.51$ and decreases with L for $p \gtrsim 0.51$. At the transition, we find that the wavefunction is area-law entangled on average, as indicated by a data collapse (inset) assuming $\nu = 0.9(4)$ and $p_{\mathrm{ctrl}} = 0.50(2)$. In Fig. 4 (right), we plot $\overline{S_A}(t)$ for $L = 10, \ldots, 18$. The results collapse as a function of $\sqrt{t/L^2}$ (see also Fig. 3) consistent with the classical expectation. In the early-time regime $t \ll L$, the realization-averaged entanglement grows diffusively, $\overline{S_A}(t, L) \sim \sqrt{t}/L$.

The entanglement properties at the transition also follow from the FDW dynamics. In the quantum model, the FDW becomes a wave packet with average position $\langle r(t) \rangle = \sum_x |\langle x|\psi(t)\rangle|^2 r_x$, where r_x is the position of the FDW in the CB state $|x\rangle$. In the quantum setting, the uncontrolled region to the right of the FDW develops entanglement due to the action of the local scrambler S_{qm} (see Fig. 1). The FDW thus constitutes a front between entangled and disentangled regions, so its dynamics govern the half-cut entanglement. At the transition the transport of the FDW is diffusive, so the entanglement dynamics must also be diffusive. Furthermore, since volume-law entanglement can only develop when the FDW "sticks" to the left edge of the chain for at least an $O(L)$ time [64], which is exponentially unlikely in an unbiased random walk, the average entanglement is at most area law at the transition.

Discussion and outlook.—In this Letter, we construct a quantum model that generalizes the stochastic dynamics associated with the probabilistic control of classical chaos. The model exhibits a dynamical entanglement transition reminiscent of MIPTs as well as a control transition that is witnessed by a local order parameter. We present an analytical argument based on the dynamics of the FDW that the entanglement and control transitions coincide, and our finite-size scaling analysis [64] finds that the two transitions are not distinguishable. Our numerical results indicate a diffusive transition at a critical control rate $p_{\mathrm{ctrl}} = 0.5 \pm 0.02$, consistent with both large-system numerics and previous analytical results for the classical version of the transition. We note, however, that the control and entanglement transitions need not coincide in general, and indeed models can be designed where the transitions are pulled apart by separately adjustable measurement and control rates [73,74]. Control transitions like the one studied here open the door to probing ordered phases and phase transitions in monitored quantum dynamics without the need for postselection onto individual quantum trajectories [75]. We therefore expect that such transitions can be observed in a variety of noisy intermediate-scale quantum experiments.

We thank Piotr Sierant for helpful comments on an earlier version of the manuscript. J. H. W. acknowledges illuminating discussions with Michael Buchhold. This work was supported in part by the National Science Foundation under Grants No. DMR-2143635 (T. I.), No. OMA-1936351 (S. G.), and No. DMR-2238895 (J. H. W). J. H. P. was supported by the Alfred P. Sloan Foundation through a Sloan Research Fellowship and the Office of Naval Research Grant No. N00014-23-1-2357. This work was initiated, performed, and completed at the Aspen Center for Physics, which is supported by the National Science Foundation Grant No. PHY-1607611.

[1] M. Foss-Feig, D. Hayes, J. M. Dreiling, C. Figgatt, J. P. Gaebler, S. A. Moses, J. M. Pino, and A. C. Potter, Holographic quantum algorithms for simulating correlated spin systems, Phys. Rev. Res. **3**, 033002 (2021).

[2] N. Tantivasadakarn, R. Thorngren, A. Vishwanath, and R. Verresen, Long-range entanglement from measuring symmetry-protected topological phases, arXiv:2112.01519.

[3] T.-C. Lu, L. A. Lessa, I. H. Kim, and T. H. Hsieh, Measurement as a shortcut to long-range entangled quantum matter, PRX Quantum **3**, 040337 (2022).

[4] A. J. Friedman, C. Yin, Y. Hong, and A. Lucas, Locality and error correction in quantum dynamics with measurement, Phys. Rev. B **107**, L220204 (2023).

[5] D. Gottesman, An introduction to quantum error correction and fault-tolerant quantum computation, arXiv:0904.2557.

[6] M. A. Nielsen and I. L. Chuang, *Quantum Computation and Quantum Information: 10th Anniversary Edition*, anniversary edition (Cambridge University Press, Cambridge, New York, 2011).

[7] H. M. Hurst and I. B. Spielman, Measurement-induced dynamics and stabilization of spinor-condensate domain walls, Phys. Rev. A **99**, 053612 (2019).

[8] H. M. Hurst, S. Guo, and I. B. Spielman, Feedback induced magnetic phases in binary Bose-Einstein condensates, Phys. Rev. Res. **2**, 043325 (2020).

[9] Y. Li, X. Chen, and M. P. A. Fisher, Quantum Zeno effect and the many-body entanglement transition, Phys. Rev. B **98**, 205136 (2018).

[10] Y. Li, X. Chen, and M. P. A. Fisher, Measurement-driven entanglement transition in hybrid quantum circuits, Phys. Rev. B **100**, 134306 (2019).

[11] B. Skinner, J. Ruhman, and A. Nahum, Measurement-Induced Phase Transitions in the Dynamics of Entanglement, Phys. Rev. X **9**, 031009 (2019).

[12] A. C. Potter and R. Vasseur, Entanglement dynamics in hybrid quantum circuits, in *Entanglement in Spin Chains* (Springer, Cham, 2022).

[13] R. Vasseur, A. C. Potter, Y.-Z. You, and A. W. W. Ludwig, Entanglement transitions from holographic random tensor networks, Phys. Rev. B **100**, 134203 (2019).

[14] Y. Bao, S. Choi, and E. Altman, Theory of the phase transition in random unitary circuits with measurements, Phys. Rev. B **101**, 104301 (2020).

[15] M. J. Gullans and D. A. Huse, Dynamical Purification Phase Transition Induced by Quantum Measurements, Phys. Rev. X **10**, 041020 (2020).

[16] C.-M. Jian, Y.-Z. You, R. Vasseur, and A. W. W. Ludwig, Measurement-induced criticality in random quantum circuits, Phys. Rev. B **101**, 104302 (2020).

[17] Y. Li, X. Chen, A. W. W. Ludwig, and M. P. A. Fisher, Conformal invariance and quantum nonlocality in critical hybrid circuits, Phys. Rev. B **104**, 104305 (2021).
[18] A. Zabalo, M. J. Gullans, J. H. Wilson, S. Gopalakrishnan, D. A. Huse, and J. H. Pixley, Critical properties of the measurement-induced transition in random quantum circuits, Phys. Rev. B **101**, 060301(R) (2020).
[19] A. Zabalo, M. J. Gullans, J. H. Wilson, R. Vasseur, A. W. W. Ludwig, S. Gopalakrishnan, D. A. Huse, and J. H. Pixley, Operator Scaling Dimensions and Multifractality at Measurement-Induced Transitions, Phys. Rev. Lett. **128**, 050602 (2022).
[20] A. Lavasani, Y. Alavirad, and M. Barkeshli, Measurement-induced topological entanglement transitions in symmetric random quantum circuits, Nat. Phys. **17**, 342 (2021).
[21] Y. Bao, S. Choi, and E. Altman, Symmetry enriched phases of quantum circuits, Ann. Phys. (Amsterdam) **435**, 168618 (2021).
[22] Y. Li and M. Fisher, Robust decoding in monitored dynamics of open quantum systems with Z_2 symmetry, arXiv:2108.04274.
[23] U. Agrawal, A. Zabalo, K. Chen, J. H. Wilson, A. C. Potter, J. H. Pixley, S. Gopalakrishnan, and R. Vasseur, Entanglement and Charge-Sharpening Transitions in U(1) Symmetric Monitored Quantum Circuits, Phys. Rev. X **12**, 041002 (2022).
[24] F. Barratt, U. Agrawal, S. Gopalakrishnan, D. A. Huse, R. Vasseur, and A. C. Potter, Field Theory of Charge Sharpening in Symmetric Monitored Quantum Circuits, Phys. Rev. Lett. **129**, 120604 (2022).
[25] M. Ippoliti, M. J. Gullans, S. Gopalakrishnan, D. A. Huse, and V. Khemani, Entanglement Phase Transitions in Measurement-Only Dynamics, Phys. Rev. X **11**, 011030 (2021).
[26] A. Lavasani, Y. Alavirad, and M. Barkeshli, Topological Order and Criticality in $(2+1)$ D Monitored Random Quantum Circuits, Phys. Rev. Lett. **127**, 235701 (2021).
[27] M. Van Regemortel, Z.-P. Cian, A. Seif, H. Dehghani, and M. Hafezi, Entanglement Entropy Scaling Transition under Competing Monitoring Protocols, Phys. Rev. Lett. **126**, 123604 (2021).
[28] N. Lang and H. P. Büchler, Entanglement transition in the projective transverse field Ising model, Phys. Rev. B **102**, 094204 (2020).
[29] S. Sang and T. H. Hsieh, Measurement-protected quantum phases, Phys. Rev. Res. **3**, 023200 (2021).
[30] S. Choi, Y. Bao, X.-L. Qi, and E. Altman, Quantum Error Correction in Scrambling Dynamics and Measurement Induced Phase Transition, Phys. Rev. Lett. **125**, 030505 (2020).
[31] O. Alberton, M. Buchhold, and S. Diehl, Entanglement Transition in a Monitored Free-Fermion Chain: From Extended Criticality to Area Law, Phys. Rev. Lett. **126**, 170602 (2021).
[32] M. Szyniszewski, A. Romito, and H. Schomerus, Entanglement transition from variable-strength weak measurements, Phys. Rev. B **100**, 064204 (2019).
[33] O. Lunt and A. Pal, Measurement-induced entanglement transitions in many-body localized systems, Phys. Rev. Res. **2**, 043072 (2020).
[34] S. Goto and I. Danshita, Measurement-induced transitions of the entanglement scaling law in ultracold gases with controllable dissipation, Phys. Rev. A **102**, 033316 (2020).
[35] Q. Tang and W. Zhu, Measurement-induced phase transition: A case study in the nonintegrable model by density-matrix renormalization group calculations, Phys. Rev. Res. **2**, 013022 (2020).
[36] X. Cao, A. Tilloy, and A. De Luca, Entanglement in a fermion chain under continuous monitoring, SciPost Phys. **7**, 024 (2019).
[37] A. Nahum, S. Roy, B. Skinner, and J. Ruhman, Measurement and entanglement phase transitions in all-to-all quantum circuits, on quantum trees, and in Landau-Ginsburg theory, PRX Quantum **2**, 010352 (2021).
[38] X. Turkeshi, R. Fazio, and M. Dalmonte, Measurement-induced criticality in $(2+1)$ -dimensional hybrid quantum circuits, Phys. Rev. B **102**, 014315 (2020).
[39] L. Zhang, J. A. Reyes, S. Kourtis, C. Chamon, E. R. Mucciolo, and A. E. Ruckenstein, Nonuniversal entanglement level statistics in projection-driven quantum circuits, Phys. Rev. B **101**, 235104 (2020).
[40] M. Szyniszewski, A. Romito, and H. Schomerus, Universality of Entanglement Transitions from Stroboscopic to Continuous Measurements, Phys. Rev. Lett. **125**, 210602 (2020).
[41] Y. Fuji and Y. Ashida, Measurement-induced quantum criticality under continuous monitoring, Phys. Rev. B **102**, 054302 (2020).
[42] D. Rossini and E. Vicari, Measurement-induced dynamics of many-body systems at quantum criticality, Phys. Rev. B **102**, 035119 (2020).
[43] S. Vijay, Measurement-driven phase transition within a volume-law entangled phase, arXiv:2005.03052.
[44] X. Turkeshi, A. Biella, R. Fazio, M. Dalmonte, and M. Schiró, Measurement-induced entanglement transitions in the quantum Ising chain: From infinite to zero clicks, Phys. Rev. B **103**, 224210 (2021).
[45] P. Sierant, G. Chiriacò, F. M. Surace, S. Sharma, X. Turkeshi, M. Dalmonte, R. Fazio, and G. Pagano, Dissipative Floquet dynamics: From steady state to measurement induced criticality in trapped-ion chains, Quantum **6**, 638 (2022).
[46] S. Sharma, X. Turkeshi, R. Fazio, and M. Dalmonte, Measurement-induced criticality in extended and long-range unitary circuits, SciPost Phys. Core **5**, 023 (2022).
[47] X. Chen, Non-unitary free boson dynamics and the boson sampling problem, arXiv:2110.12230.
[48] Y. Han and X. Chen, Measurement-induced criticality in Z 2 -symmetric quantum automaton circuits, Phys. Rev. B **105**, 064306 (2022).
[49] J. Iaconis, A. Lucas, and X. Chen, Measurement-induced phase transitions in quantum automaton circuits, Phys. Rev. B **102**, 224311 (2020).
[50] M. Buchhold, Y. Minoguchi, A. Altland, and S. Diehl, Effective Theory for the Measurement-Induced Phase Transition of Dirac Fermions, Phys. Rev. X **11**, 041004 (2021).
[51] B. Ladewig, S. Diehl, and M. Buchhold, Monitored Open Fermion Dynamics: Exploring the Interplay of Measurement, Decoherence and Free Hamiltonian Evolution, Phys. Rev. Res. **4**, 033001 (2022).

[52] T. Müller, S. Diehl, and M. Buchhold, Measurement-Induced Dark State Phase Transitions in Long-Ranged Fermion Systems, Phys. Rev. Lett. **128**, 010605 (2022).
[53] A. Altland, M. Buchhold, S. Diehl, and T. Micklitz, Dynamics of measured many-body quantum chaotic systems, Phys. Rev. Res. **4**, L022066 (2022).
[54] J. Willsher, S.-W. Liu, R. Moessner, and J. Knolle, Measurement-induced phase transition in a chaotic classical many-body system, Phys. Rev. B **106**, 024305 (2022).
[55] F. Barratt, U. Agrawal, A. C. Potter, S. Gopalakrishnan, and R. Vasseur, Transitions in the Learnability of Global Charges from Local Measurements, Phys. Rev. Lett. **129**, 200602 (2022).
[56] J. Côté and S. Kourtis, Entanglement Phase Transition with Spin Glass Criticality, Phys. Rev. Lett. **128**, 240601 (2022).
[57] P. Sierant and X. Turkeshi, Universal Behavior beyond Multifractality of Wave Functions at Measurement-Induced Phase Transitions, Phys. Rev. Lett. **128**, 130605 (2022).
[58] M. McGinley, S. Roy, and S. A. Parameswaran, Absolutely Stable Spatiotemporal Order in Noisy Quantum Systems, Phys. Rev. Lett. **129**, 090404 (2022).
[59] Y. Herasymenko, I. Gornyi, and Y. Gefen, Measurement-driven navigation in many-body Hilbert space: Active-decision steering, arXiv:2111.09306.
[60] E. Ott, C. Grebogi, and J. A. Yorke, Controlling Chaos, Phys. Rev. Lett. **64**, 1196 (1990).
[61] I. Antoniou, V. Basios, and F. Bosco, Probabilistic control of chaos: The β-adic Renyi map under control, Int. J. Bifurcation Chaos Appl. Sci. Eng. **06**, 1563 (1996).
[62] I. Antoniou, V. Basios, and F. Bosco, Absolute controllability condition for probabilistic control of chaos, Int. J. Bifurcation Chaos Appl. Sci. Eng. **08**, 409 (1998).
[63] I. Antoniou, V. Basios, and F. Bosco, Probabilistic control of Chaos: Chaotic maps under control, Comput. Math. Appl. **34**, 373 (1997).
[64] See Supplemental Material at http://link.aps.org/supplemental/10.1103/PhysRevLett.131.060403, which contains Refs. [64,65], for further discussions of the classical control transition, the relationship between the classical and quantum formulations of the Bernoulli map, and additional data on the quantum model corroborating statements made in the main text.
[65] D. N. Page, Average Entropy of a Subsystem, Phys. Rev. Lett. **71**, 1291 (1993).
[66] N. Kawashima and N. Ito, Critical behavior of the three-dimensional $\pm j$ model in a magnetic field, J. Phys. Soc. Jpn. **62**, 435 (1993).
[67] A. Rényi, Representations for real numbers and their ergodic properties, Acta Math. Acad. Sci. Hung. **8**, 477 (1957).
[68] S. Takesue, Ergodic properties and thermodynamic behavior of elementary reversible cellular automata. I. Basic properties, J. Stat. Phys. **56**, 371 (1989).
[69] S. Gopalakrishnan and B. Zakirov, Facilitated quantum cellular automata as simple models with non-thermal eigenstates and dynamics, Quantum Sci. Technol. **3**, 044004 (2018).
[70] T. Iadecola and S. Vijay, Nonergodic quantum dynamics from deformations of classical cellular automata, Phys. Rev. B **102**, 180302(R) (2020).
[71] M. Émile Borel, Les probabilités dénombrables et leurs applications arithmétiques, Rend. Circ. Mat. Palermo **27**, 247 (1909).
[72] M. J. Gullans and D. A. Huse, Scalable Probes of Measurement-Induced Criticality, Phys. Rev. Lett. **125**, 070606 (2020).
[73] V. Ravindranath, Y. Han, Z.-C. Yang, and X. Chen, Entanglement steering in adaptive circuits with feedback, arXiv:2211.05162.
[74] N. O'Dea, A. Morningstar, S. Gopalakrishnan, and V. Khemani, Entanglement and absorbing-state transitions in interactive quantum dynamics, arXiv:2211.12526.
[75] A. J. Friedman, O. Hart, and R. Nandkishore, Measurement-induced phases of matter require adaptive dynamics, arXiv:2210.07256.